Journal of Organometallic Chemistry, 341 (1988) 523–534
Elsevier Sequoia S.A., Lausanne – Printed in The Netherlands

Molecular orbital analysis of some carbonyl cluster compounds with close-packed metallic arrangements *

D. Michael P. Mingos* and Lin Zhenyang

Inorganic Chemistry Laboratory, University of Oxford, South Parks Road, Oxford OX1 3QR (Great Britain)

(Received October 20th, 1987)

Abstract

The bonding in a series of rhodium carbonyl cluster compounds with $12n_s + 24$ valence electrons, where n_s is the number of surface rhodium atoms, has been analyzed using a combination of Extended Hückel Molecular Orbital Calculations and symmetry arguments derived from Stone's Tensor Surface Harmonic Theory. In addition, a comparison has been made between the alternative close-packing possibilities for 13-atom metallic clusters.

Introduction

During the last twenty years, simplified bonding schemes derived primarily from symmetry arguments and semi-empirical molecular orbital calculations have been developed and have provided a rudimentary understanding of the electronic structures of transition metal cluster compounds [1,2]. The *isolobal* analogy [3] and Stone's Tensor Surface Harmonic Methodology [4] have been particularly useful for providing a theoretical framework for the cluster compounds of the transition and main group elements. The cluster compounds $[Rh_{13}(CO)_{24}H_{5-x}]^{x-}$ and $[Rh_{15}(CO)_{30}]^{3-}$ [5,6] provide particularly good examples of the usefulness of these theoretical concepts. In both cases, the clusters have a central interstitial rhodium atom, and remaining metal atoms define a four-connected polyhedron, an anticuboctahedron in the former case and a rhombohedron in the latter. The metal atoms lie on a single spherical surface and, using the Stone methodology, we have previously demonstrated that spherical 4-connected clusters are characterised by $14n_s + 2$ valence electrons [7] i.e. they have $n_s + 1$ occupied bonding skeletal molecular orbitals, where n_s is the number of surface metal atoms. Therefore, these spherical 4-connected clusters have been the same number of bonding skeletal molecular orbitals as deltahedral clusters.

* Dedicated to Professor Colin Eaborn on the occasion of his 65th birthday.

0022-328X/88/$03.50

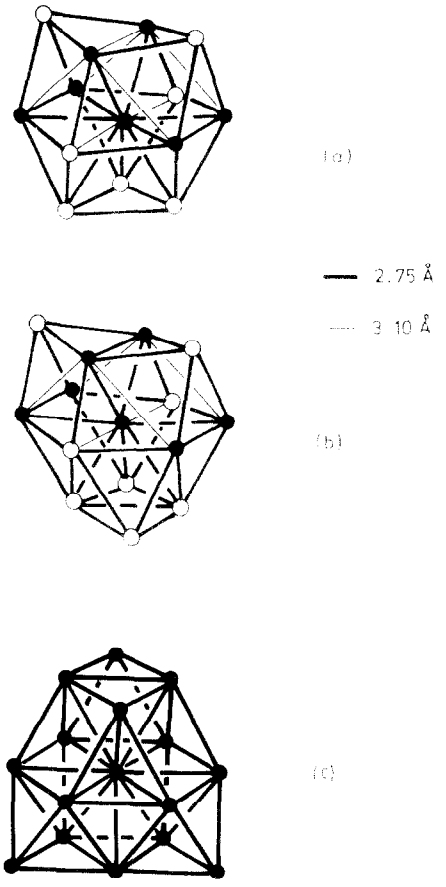

Fig. 1. Structures of (a) $[Rh_{14}(CO)_{25}]^{4-}$, (b) $[Rh_{15}(CO)_{27}]^{3-}$ and (c) $[Rh_{17}(CO)_{30}]^{3-}$ anions.

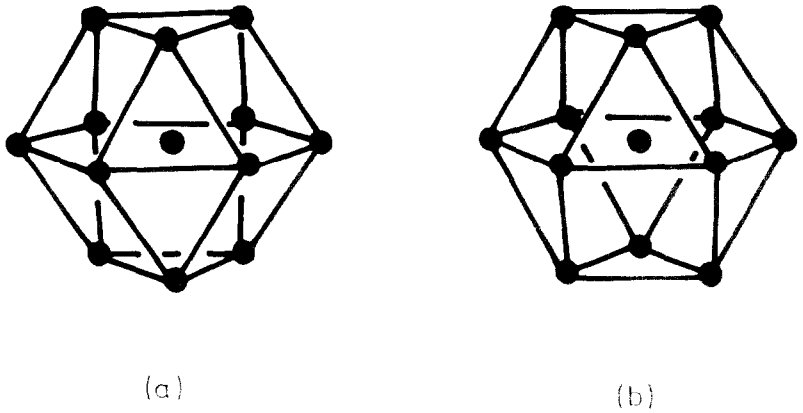

Fig. 2. Structures of (a) the anti-cuboctahedron and (b) the cuboctahedron.

Table 1

High nuclearity carbonyl cluster compounds with the electron count $12n_s + 24$ [a]

Compound	n_i [b]	n_s [b]	Total number of valence electrons	
$[Rh_{14}(CO)_{25}]^{4-}$	1	13	180	$12n_s + 24$
$[Rh_{14}(CO)_{26}]^{2-}$	1	13	180	
$[Rh_{15}(CO)_{27}]^{3-}$	1	14	192	
$[Rh_{17}(CO)_{30}]^{3-}$	1	16	216	
$[Rh_{13}(CO)_{24}H_{5-x}]^{x-}$	1	12	170	$12n_s + 2(n_s + 1)$
$[Rh_{15}(CO)_{30}]^{3-}$	1	14	198	

[a] From Ref. 1. [b] n_i = number of interstitial metal atoms; n_s = number of surface metal atoms.

The $[Rh_{13}(CO)_{24}H_{5-x}]^{x-}$ clusters have a close-packed arrangement of metal atoms which corresponds to the primary fragment of a hexagonal close-packed (h.c.p.) metal structure, i.e. the metal atoms define an anti-cuboctahedron. There are, however, some rhodium clusters which are structurally related to $[Rh_{13}(CO)_{24}H_{5-x}]^{x-}$, but do not conform to the simple bonding patterns described above for spherical rhodium clusters. Figures 1a and 1b illustrate the structures of $[Rh_{14}(CO)_{25}]^{4-}$ and $[Rb_{15}(CO)_{27}]^{3-}$ [8]. The latter is related to the former by the incorporation of an additional metal capping atom over a square face. $[Rh_{14}(CO)_{26}]^{2-}$ is isoelectronic with $[Rh_{14}(CO)_{25}]^{4-}$ and has a very similar skeletal geometry. These Rh_{14} and Rh_{15} clusters do not have very symmetrical structures, and can be related to either the cuboctahedron and anti-cuboctahedron shown in Fig. 2. Consequently, they can be described as fragments of either face-centered cubic (f.c.c.) or h.c.p. metallic structures. The $[Rh_{17}(CO)_{30}]^{3-}$ [9] ion has a more symmetrical structure, based on a tetracapped anti-cuboctahedron (see Fig. 1c). Interestingly, these clusters are all associated with $12n_s + 24$ valence electrons (see Table 1), suggesting the occurrence of twelve skeletal molecular orbitals. These clusters do not, therefore, conform to a simple spherical model which would result in the occupation of $n_s + 1$ bonding skeletal molecular orbitals, or to a bispherical model [10] which would recognise the location of several metal atoms in capping positions. According to the *capping principle* [11], capped structures based on either the cuboctahedron or the anti-cuboctahedron should be associated with thirteen skeletal bonding molecular orbitals. In order to provide some insight into these exceptions to the Polyhedral Skeletal Electron Pair Theory [12], we have completed extended Hückel molecular orbital calculations on the compounds illustrated in Fig. 1.

Results and discussion

We have completed extended Hückel molecular orbital calculations on the centred cuboctahedral (f.c.c.) and the anti-cuboctahedral (h.c.p.) forms of $Rh_{13}H_{36}$ derived from RhH_3 fragments. The results are illustrated in Figs. 3 and 4. The non-bonding "t_{2g}" orbitals and the M–L bonding molecular orbitals have been omitted from these figures for reasons of clarity. Figure 3 shows the interactions between the surface atoms of the cuboctahedron and the central atom. The skeletal molecular orbitals for the surface atoms of the cuboctahedron lie in a narrow energy

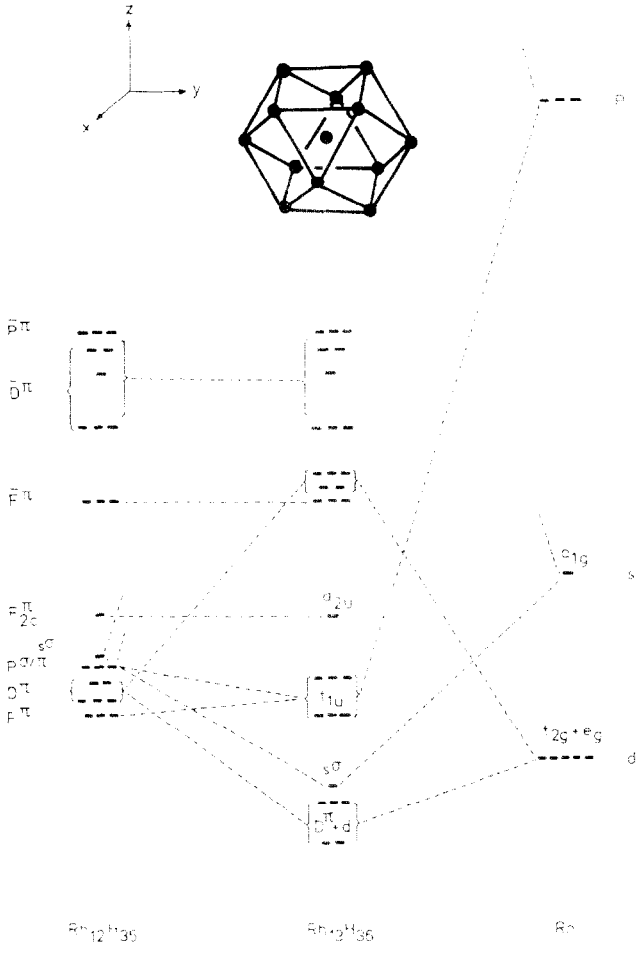

Fig. 3. MO interaction diagram for a centred cuboctahedron.

range and comprise $F^{\pi}(t_{1u})$, $D^{\pi}(t_{2g}+e_g)$, $P^{\sigma/\pi}(t_{1u})$, S^{σ} and $F^{\pi}_{2c}(a_{2u})$ (the z axis is defined along the 4-fold axis). There are a total of thirteen skeletal bonding molecular orbitals. This is a general characteristic of 4-connected clusters and this aspect has been discussed in some detail elsewhere [11]. When the central atom is inserted into the Rh_{12} cluster, the three p orbitals of the central atom stabilize the $P^{\sigma/\pi}$ orbitals slightly. The s and d orbitals interact strongly with the S^{σ} and D^{π} orbitals of the outer sphere, and give rise to the in-phase combinations $S^{\sigma}+s$ and $D^{\pi}+d$ bonding orbitals, and the out-of-phase combinations $S^{\sigma}-s$ and $D^{\pi}-d$, which are antibonding. The F^{π} orbitals are essentially unaffected by the introduction of the central atom. Consequently, the interaction between s, p and d orbitals of the interstitial atom and the skeletal bonding orbitals of the outer sphere leads to no change in the total number of the skeletal bonding orbitals.

Figure 4 shows a correlation diagram of the energy levels for the interconversion of cuboctahedral and anti-cuboctahedral structures. It can be seen that both structures have the same number and similar patterns in their skeletal molecular

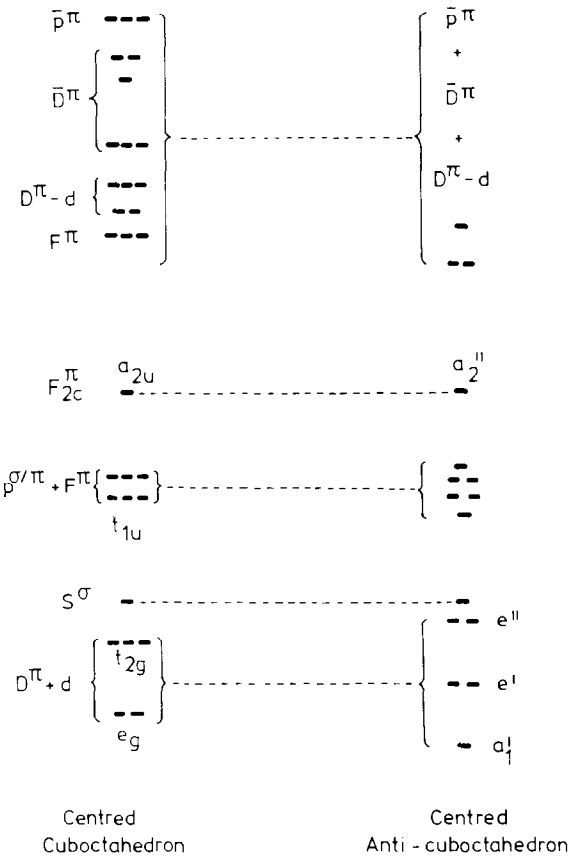

Fig. 4. The correlation MO diagram of the centred cuboctahedron and the centred anti-cuboctahedron.

orbitals. Moreover, the HOMOs F_{2c}^{π} which are illustrated in Fig. 5 have nearly the same energy. It can be seen form Fig. 5 that the F_{2c}^{π} wavefunction has regular nodal characteristics. For the cuboctahedron, the square faces have δ local symmetry characteristics and the triangular faces have σ local symmetry characteristics. The F_{2c}^{π} wavefunction for the anti-cuboctahedron has very similar nodal characteristics.

It is apparent that the F_{2c}^{π} molecular orbital (see Fig. 3) is higher lying than the other F^{π} components, and there is a big gap between HOMO and the next stable molecular orbital. This is because there is no F_{2c}^{σ} wavefunction for either a cuboctahedron or an anti-cuboctahedron, and the F_{2c}^{π} cannot be stabilized by mixing with the σ wavefunction. In Table 2, the L^{π} and L^{σ} wavefunctions for different types of close packings based on twelve metal atoms lying on the surface of a pseudo-spherical symmetry are listed. For the cuboctahedron, the anti-cuboctahedron, and tetracapped cube, there is one F_2^{π} function which is not matched by a F_2^{σ} function, and consequently cannot be stabilised by σ/π mixing. These clusters are showing a deficiency of the Stone methodology, which results from their deviation from spherical symmetry. The lack of σ/π mixing causes a significant removal of the degeneracy of the F^{π} functions.

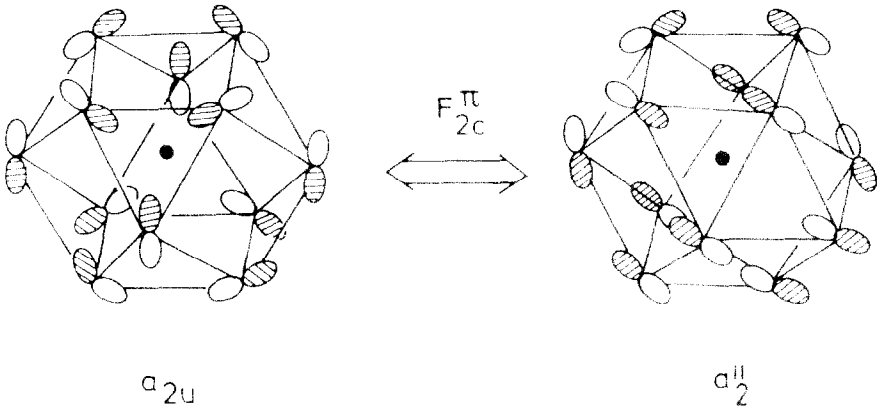

Fig. 5. The F^{π}_{2c} wavefunctions for cuboctahedron and anti-cuboctahedron.

Usually, the frontier orbitals or a capping fragment have σ and π pseudo-symmetries; for example, the ML_3 fragment has $a_1 + e$ frontier orbitals. Therefore, the F^{π}_{2c} wavefunction for the cuboctahedron cluster does not interact with the frontier orbitals of the capping fragment when the square faces are capped because of its δ character, but it does interact with the "t_{2g}" set of the capping fragment which has δ character and is destabilized slightly. The result of MO calculations, shown in Fig. 6, on the centred cuboctahedron with two ML_3 fragments capping the two square faces which are perpendicular to the z axis (see Fig. 3 for the coordinate system) confirms this conclusion. The frontier orbitals ($e' + e''$) of the two fragments, which interact strongly with both the skeletal bonding molecular orbitals (shown in Fig. 6) and the "t_{2g}" non-bonding orbitals (omitted from the Figure) of the centred cuboctahedral cluster, are destabilized and become more antibonding. Therefore, capping the square faces of the parent cluster leads to a net destabilisation of the F^{π}_{2c} molecular orbital. When more capping atoms are introduced, the F^{π}_{2c} is destabilized even further. Consequently, the F^{π}_{2c} molecular orbital may become unavailable when the number of capping atoms increases, because of its high lying nature and destabilization by the "t_{2g}" set of the capping fragments. The $[Rh_{17}(CO)_{30}]^{3-}$ cluster with twelve skeletal electron pairs (SEPs) rather than 13 SEPs, which is derived from the regular anti-cuboctahedron by capping four of the six square faces, provides an example of this bonding situation. We have previously noted that the introduction of several capping atoms can result in the introduction of additional skeletal molecular orbitals localized predominantly on the capping atoms, where the symmetries do not match those of the bonding skeletal MOs of the parent polyhedron. This bonding analysis provides the first example of the number of skeletal MOs being decreased by capping, and is a direct consequence of the local δ character of the F^{π}_{2c} molecular orbital and the absence of a matching F^{σ}_{2c} molecular orbital.

When there are one or two capping atoms, the F^{π}_{2c} is not destabilized as much (see Fig. 6). This implies that another factor contributes to the unavailability of the F^{π}_{2c} orbital in the Rh_{14} and Rh_{15} clusters. A close examination of their structures has established that they are based on a very distorted cuboctahedron or anti-cuboctahedron. As a result of the distortion, the distances between the diagonal atoms in

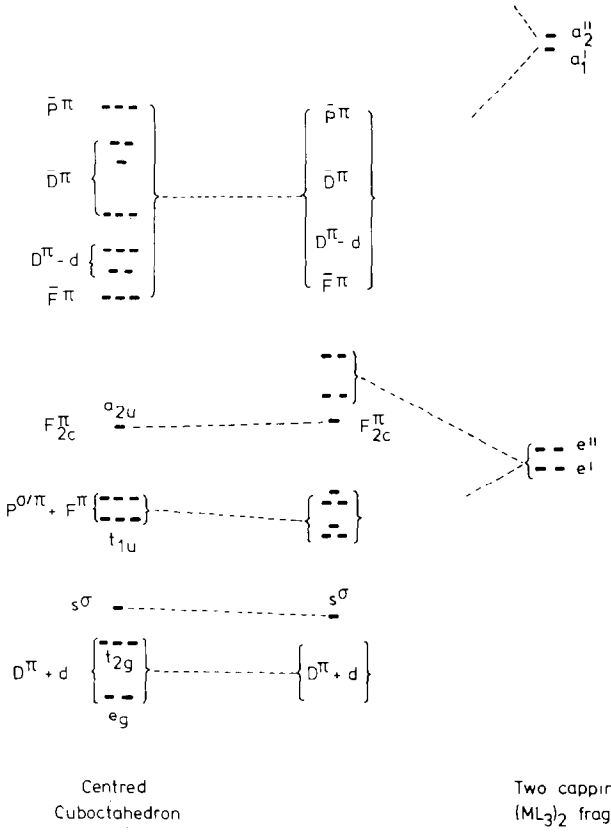

Fig. 6. MO interaction diagram for a centred cuboctahedron with two capping fragments.

the square faces becomes much shorter (ca. 3.1 Å) than that for a regular square face in both h.c.p. and f.c.c. (ca. 3.9 Å). In the unit cell for h.c.p. or f.c.c., each atom is surrounded by twelve equidistant nearest neighours. In the unit cell for body-centered cubic (b.c.c.), each atom is surrounded by eight nearest neighbours, and there are six other atoms which are only slightly further away. The structure illustrated in Fig. 1 indicate that there are nine nearest neighbours surrounding the central atom in these two clusters. The black balls in Fig. 1 indicate that they correspond to a part of b.c.c. packing. The discussions above show that the structures illustrated in Fig. 1 are intermediate between b.c.c. and h.c.p. or f.c.c. close packing, rather than being pure h.c.p., f.c.c. or b.c.c.

The cuboctahedron may be viewed as an elongated cube with four atoms capping the four rectangular faces. Therefore, the distorted cuboctahedron can be derived from the tetra-capped cube (the primary polyhedron of b.c.c. close packing). The correlation diagram of energy levels for this transformation is illustrated in Fig. 7. It is apparent that the F^{π}_{2c} is destabilized when the cuboctahedron is compressed along the four-fold axis because the antibonding character increases (the wavefunction of the F^{π}_{2c} molecular orbital is shown in Fig. 5). Therefore, such a distortion can raise the energy of the F^{π}_{2c} orbital sufficiently to make it unavailable for bonding. The

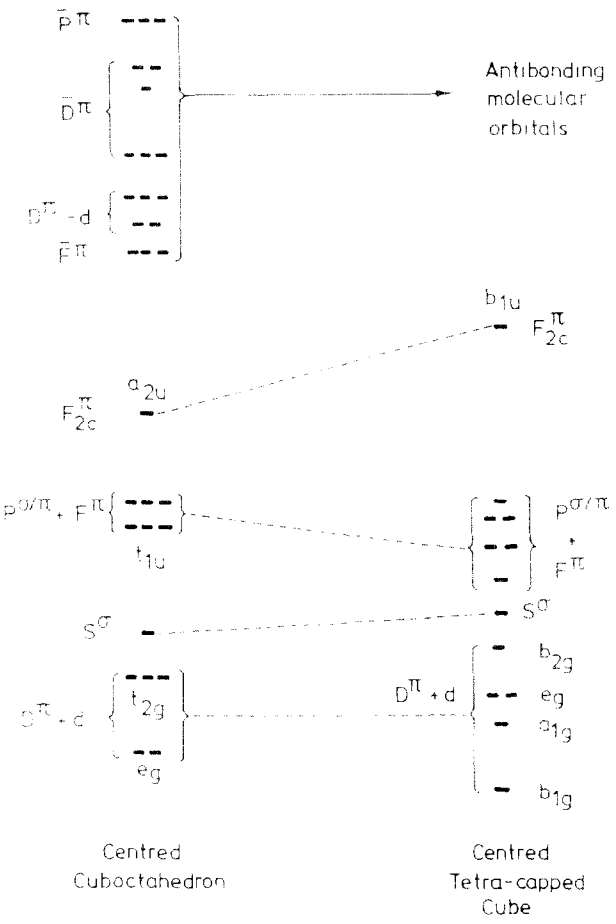

Fig. 7. The correlation MO diagram of the centred cuboctahedron and the centred tetra-capped cube.

deviation from the spherical geometry caused by distortion raises the energy of F_{2c}^{π} because, for a cube, this orbital is skeletal anti-bonding and only stabilized by the effects of the capping atoms.

In summary, there are two factors resulting in the unavailability of the high lying skeletal bonding orbital F_{2c}^{π}. One is the δ character of F_{2c}^{π} in the capping faces, and the other is the distortion away from spherical symmetry. For the larger clusters, the former predominates because of the strong interaction between the F_{2c}^{π} orbital and the "t_{2g}" set from the capping fragments. For the smaller clusters, the later predominates.

The comparisons between four different types of close-packed arrangements

The structures of high nuclearity clusters arise form the vertex, edge and face sharing of smaller polyhedral units. Extensive condensation of these smaller polyhedral clusters leads to packing arrangements which are related to b.c.c., h.c.p. and

f.c.c. metallic lattices. The observed structures in Table 1 can be described either in terms of these idealized close-packed arrangements, or as intermediate structures. We have completed a theoretical analysis on these different types of close-packing, using the prototypic centred clusters with thirteen metal atoms. They are the anti-cuboctahedron (b.c.p.), cuboctahedron (f.c.c.), tetra-capped cube (b.c.c.), and also the icosahedron which forms the basis of icosahedral close packing (i.c.p.). Table 3 summarizes the results of MO calculations on these four structures with and without the central atom.

1. Comparison between the frontier orbitals

Table 2 lists the all L^{σ} and L^{π} wavefunctions for the four typical structures. It can be seen from the Table that the L^{σ} and L^{π} wavefunctions for anti-cuboctahedron, cuboctahedron and tetra-capped cube follow a similar pattern. As discussed above, the F^{π}_{2c} orbital is an unavailable molecular orbital for the tetra-capped cube (see Fig. 7), but occupied for the anti-cuboctahedron and cuboctahedron, resulting in a total of $n+1$ skeletal bonding molecular orbitals. In these three close-packed arrangements, the F^{π}_{2c} orbital cannot be stabilized through σ and π mixing. Consequently, this orbital is always the frontier orbital. For the icosahedron, the four $F^{\pi}_{\pm 1,\pm 2}$ orbitals cannot gain any stabilization through σ and π mixing since the $F^{\sigma}_{0,\pm 3}$ wavefunctions have different symmetry transformation properties. Therefore, the $F^{\pi}_{\pm 1,\pm 2}$ orbitals are high lying. The MO calculations have confirmed that the $F^{\pi}_{\pm 1,\pm 2}(g_u)$ molecular orbitals are the HOMOs. As a result of the presence of these four high lying orbitals, the total energy for the icosahedron is less favourable than those for the others (see Table 3). The calculations suggest that the h.c.p. and f.c.c. structures are more stable. This provides a rationalization for the absence of an icosahedral Rh_{13} cluster. In the clusters where the π tangential skeletal bonding orbitals are not important and the high lying $F^{\pi}_{\pm 1,\pm 2}$ orbitals are unoccupied, the structure may adopt an icosahedral close-packed arrangement. For example, $[Au_{13}Cl_2(PMe_2Ph)_{10}]^{3+}$ which is characterized by a $12n_s + 18$ electron count [5,12] has an icosahedral structure because radial bonding predominates.

Table 2

The wavefunctions of L^{σ} and L^{π} of Rh_{13} for different types of spherical close-packed arrangements

Structure	Function	
	nL^{π}	nL^{σ}
anti-cuboctahedron	$P^{\pi}(a_2+e)$,	S^{σ}, $P^{\sigma}(a_2+e)$,
	$D^{\pi}(a_1+e+e)$	$D^{\sigma}(a_1+e+e)$
(h.c.p.)	$F^{\pi}(a_1+e)$, $F^{\pi}(a_2)$	$F^{\sigma}(a_1+e)$
cuboctahedron	$P^{\pi}(t_{1u})$, $D^{\pi}(e_g+t_{2g})$	S^{σ}, $P^{\sigma}(t_{1u})$, $D^{\sigma}(e_g+t_{2g})$
(f.c.c.)	$F^{\pi}(t_{1u})$, $F^{\pi}_{2c}(a_{2u})$	$F^{\sigma}(t_{1u})$
tetra-capped cube	$P^{\pi}(a_{2u}+e_u)$,	S^{σ}, $P^{\sigma}(a_{2u}+e_u)$,
	$D^{\pi}(a_{1g}+b_{1g}+b_{2g}+e_g)$	$D^{\sigma}(a_{1g}+b_{1g}+b_{2g}+e_g)$
(b.c.c.)	$F^{\pi}(a_{2u}+e_u)$, $F^{\pi}_{2c}(b_{1u})$	$F^{\sigma}(a_{2u}+e_u)$
icosahedron	$P^{\pi}(t_{1u})$, $D^{\pi}(h_g)$	S^{σ}, $P^{\sigma}(t_{1u})$, $D^{\sigma}(h_g)$
(i.c.p.)	$F^{\pi}_{\pm 1,\pm 2}(g_u)$	$F^{\sigma}_{0,\pm 3}(t_{2u})$

[a] The wavefunctions are labelled as for the cuboctahedron.

Table 3

Results of EHMO calculations on different types of close-packings for $Rh_{13}H_{36}$, with thirteen skeletal bonding orbitals

Structure	$D^{\pi} - d$ overlap integrals	Total energies (eV)			Number of edges (e)	Reduced overlap populations				
		without central atom (E_1)	with central atom (E_2)	$E_1 - E_2$		Rh_i–Rh [c]	Rh–Rh (M_1) without Rh_i	Rh–Rh (M_2) with Rh_i	total difference $e \cdot (M_1 - M_2)$	
anti-cuboctahedron (h.c.p.)	0.11	−2275.3	−2293.2	17.9	24	0.30	0.290	0.235	1.32	
cuboctahedron (f.c.c.)	0.13	−2274.7	−2292.6	17.9	24	0.30	0.290	0.232	1.39	
icosahedron (i.c.p.)	0.16	−2274.1	−2291.6	17.5	30	0.32	0.230	0.180	1.50	
tetra-capped cube [a,b] (b.c.c.)	0.12	−2264.2	−2279.8	15.6	16	0.38	0.260	0.230	0.48	1.20
					12	0.08	0.210	0.150	0.72	

[a] 12 skeletal bonding orbitals for b.c.c. packing. [b] There are two kinds of bond lengths for Rh_i–Rh and Rh–Rh. [c] Rh_i, the central rhodium atom; Rh, the surface rhodium atoms.

2. Effect of the central atom

The interaction between the surface atoms for each of the four structures and the central atom leads to a stabilization of S^{σ}, $P^{\sigma/\pi}$ and D^{π} skeletal bonding molecular orbitals, because they have the same symmetries as the valence orbitals of the central atom [12]. The $D^{\pi} - d$ overlap integrals in Table 3 indicate that the interaction between the central atom and the surface atoms for the icosahedron is larger than for the other structures. However, the stabilization resulting from the interaction for i.c.p. (17.5 eV) is less than those for f.c.c. and h.c.p. (17.9 eV) (see Table 3). This implies that the interaction between d valence orbitals and "t_{2g}" set from surface fragments is larger for i.c.p. This type of interaction behaves similar to $d - d$ electron repulsion effects. The insertion of the central atom also leads to the largest decrease in the total reduced overlap population between the surface atoms for i.c.p. (1.50). The larger repulsion between d electrons of the central atom and d electrons from the surface atoms accounts for the absence of Rh_{13} clusters based on icosahedral close-packing. The absence of d electrons from the central atom excludes these $d - d$ repulsions. Therefore, there is one example of icosahedral structure, $[Rh_{12}Sb(CO)_{27}]^{3-}$ [13], with a main group central atom, antimony.

For the tetra-capped cube, the decrease in the total reduced overlap populations between the surface atoms is the least, although the stabilization energy is the smallest (15.6 eV) when the central atom is inserted. From the stabilization energies in Table 3, it is apparent that the h.c.p. and f.c.c. structures are preferred; from the reduced overlap population considerations between the surface atoms, the b.c.c. structure is preferred. As the result of these two factors, therefore, the observed structures in Table 1 tend to be intermediate between b.c.c. and h.c.p. or f.c.c. The energy difference curve between h.c.p. and f.c.c., computed from the method of moments by Burdett [14] for infinite structures, is very flat. From Table 3, it is apparent that there is little difference between f.c.c. and h.c.p. for molecular clusters.

In summary, there are two factors resulting in the absence of a icosahedral structure for the Rh_{13} cluster. One is the four high lying $F^{\pi}_{\pm 1,\pm 2}$ orbitals, because of the absence of the symmetry-adapted $F^{\sigma}_{\pm 1,\pm 2}$ wavefunctions. The other is the strongly $d - d$ repulsion between the central atom and the surface atoms. The occurrence of $[Au_{13}Cl_2(PMe_2Ph)_{10}]^{3+}$ and $[Rh_{12}Sb(CO)_{27}]^{3-}$ indicates that the absence of either of these two factors leads to the occurrence of icosahedral structures.

Acknowledgements

The S.E.R.C. and the Chinese Academy of Sciences are thanked for their financial support.

Appendix

The calculations were performed within the Extended Hückel method [15]. The exponents of Rh were taken from literature [16]. $H_{ii}(s)$ -9.59 eV and $H_{ii}(p)$ -4.57 eV for Rh atoms. $H_{ii}(d)$ -12.5 eV for the surface Rh atoms and $H_{ii}(d)$ -11.0 eV for the central Rh atom. The following bond distances were used: Rh–Rh 2.75, Rh–H 1.80 Å.

References

1 (a) K. Wade, Adv. Inorg. Chem. Radiochem., 18 (1976) 1; (b) D.M.P. Mingos, Nature (London), Phys. Sci., 236 (1972) 99.
2 D.M.P. Mingos, Chem. Soc. Rev., 15 (1986) 31 and references therein.
3 (a) M. Elian and R. Hoffmann, Inorg. Chem., 14 (1975) 1058; (b) M. Elian, M.M.-L. Chen, D.M.P. Mingos, and R. Hoffmann, Inorg. Chem., 15 (1976) 1148.
4 A.J. Stone, Mol. Phys., 41 (1980) 1339; Inorg. Chem., 20 (1981) 563.
5 D.M.P. Mingos, J. Chem. Soc., Chem. Commun., (1985) 1352.
6 D.M.P. Mingos, and M.I. Forsyth, J. Chem. Soc., Dalton Trans., (1977) 610.
7 V.G. Albano, G. Ciani, S. Martinengo, and A. Sironi, J. Chem. Soc., Dalton Trans., (1979) 978.
8 P. Chini, J. Organomet. Chem., 200 (1980) 37.
9 S. Martinengo, G. Ciani, and A. Sironi, J. Chem. Soc., Chem. Commun., (1980) 1140.
10 G. Ciani, A. Magni, A. Sironi, and S. Martinengo, J. Chem. Soc., Chem. Commun., (1981) 1280.
11 R.L. Johnston, and D.M.P. Mingos, J. Chem. Soc., Dalton Trans., (1987), 647, 1445.
12 D.M.P. Mingos, and Lin Zhenyang, J. Chem. Soc., Dalton Trans., in press.
13 J.L. Vidal and J.M. Troup, J. Organomet. Chem., 213 (1981) 351.
14 J.K. Burdett, and S. Lee, J. Am. Chem. Soc., 107 (1985) 3063.
15 (a) R. Hoffmann, J. Chem. Phys., 39 (1963) 1397; (b) R. Hoffmann, and W.N. Lipscomb, ibid., 36 (1962) 2179, 3189; 37 (1962) 2872.
16 R.H. Summerville, and R. Hoffmann, J. Am. Chem. Soc., 98 (1976) 7240.